Spectral-element based 3D elastic full-waveform inversion of surface waves in the presence of complex topography using an envelope-based misfit function

Dmitry Borisov[1], Ryan Modrak[1], Herurisa Rusmanugroho[1], Yanhua O.Yuan[1], Fuchun Gao[2], Frederik J. Simons[1], and Jeroen Tromp[1], [1]Princeton University, [2]Total E&P Research and Technology*

Summary

Full-waveform inversion (FWI) is a data fitting technique used to estimate properties of the Earth from seismic data by minimizing the misfit between observed and simulated seismograms. Because of very high computational cost, this technique has so far been used either in a 2D fully elastic formulation or in a 3D acoustic formulation, when applied to active-source surveys in order to image the shallow subsurface (i.e., down to the first few kilometers). However, the Earth is three-dimensional, (visco)elastic and highly heterogeneous. Therefore, obtaining more accurate models requires solving the full 3D elastic wave equation. In this study, we use an envelope-based misfit function to construct shallow 3D models of shear wavespeed while inverting surface waves. The envelope-based misfit function has proven to be effective for inverting surface waves, which are particularly exposed to the cycle-skipping problem. To accurately model the wavefield in the presence of complex topography, we use a spectral-element wave propagation code. A synthetic example on the SEAM Phase II foothills model illustrates that inversion of surface waves at the initial stages in such a challenging environment allows us to obtain an improved shear wavespeed starting model for traditional FWI.

Introduction

Full-waveform inversion (FWI), introduced by Lailly (1983) and Tarantola (1984), is a data fitting approach to estimating elastic parameters of the Earth (e.g., compressional and/or shear wavespeeds) from seismic data. The main goal consists of minimizing the data difference between observed and synthetic seismograms through a local optimization process. The gradient of the data misfit for the model update at each iteration is efficiently calculated using the adjoint-state method (Chavent, 1974). Compared to first-arrival traveltime tomography, FWI wavespeed models generally have better resolution, which often leads to a better-migrated image. However, because of the ill-posed and highly non-linear character of the seismic inversion, the technique often suffers from cycle-skipping as a result of an inaccurate starting model and/or lack of reliable low-frequency information in the data (Virieux and Operto, 2009).

In land surveys, seismic traces recorded at the surface are dominated by high-amplitude and dispersive surface waves. Rather than removing them from the data (e.g., via an FK-filter or simply muting them, as is frequently done in the seismic exploration community), we prefer to use surface waves as an additional source of information on near-subsurface structure. However, inversion of these waveforms makes conventional waveform-difference (WD) FWI highly sensitive to the initial model due to the increased nonlinear behavior of the misfit function. Here we extend the approach of Yuan et al. (2015) to 3D geometry, in which an envelope-difference (ED) misfit function is used for inverting surface waves in the early stages of the inversion to improve shallow constraints on *P* and *S* wavespeeds. We demonstrate that the reliable near-surface velocity model allows us to better reconstruct the deeper structure in the later stages, when inverting body waves using a WD misfit function.

To demonstrate our approach, we perform 3D elastic FWI on the synthetic 3D SEAM Phase II foothills model (Oristaglio, 2012). To handle strong variations in topography, we use a solver based on the spectral-element method (Komatitsch and Vilotte, 1998; Komatitsch and Tromp, 1999), which allows for accurate wavefield simulations in the context of complex geological settings.

Envelope-based waveform inversion

First we recapitulate what the envelope of a signal is. Envelopes have shown to yield good measures of misfit in seismic inverse problems (e.g., Bozdağ et al., 2011; Wu et al., 2014). A signal with no negative-frequency components is called an analytic signal $\tilde{f}(t)$ if it is constructed from a real signal *f(t)* and its Hilbert transform *H{f(t)}*:

$$\tilde{f}(t) = f(t) + iH\{f(t)\} = E(t)e^{i\phi(t)},$$

where $\phi(t)$ is the instantaneous phase

$$\phi(t) = \arctan\frac{\Im\{\tilde{f}(t)\}}{\Re\{\tilde{f}(t)\}},$$

and *E(t)* is the instantaneous amplitude or envelope

$$E(t) = \sqrt{\Re\{\tilde{f}(t)\}^2 + \Im\{\tilde{f}(t)\}^2}.$$

The conventional least-squares waveform-difference misfit function between observed $d(x_r,x_s,t;m)$ and synthetic $s(x_r,x_s,t;m)$ data can be defined as:

$$\chi_W(m) = \frac{1}{2}\sum_{s,r}\int_0^T \left\| s(x_r,x_s,t;m) - d(x_r,x_s,t) \right\|^2 dt,$$

where T is a recording time and summation is over each source and receiver pair. The corresponding expression for the source of the adjoint wavefield can be written as:

$$f_W^\dagger(x,t) = \sum_r \left[s(x,t;m) - d(x,t) \right] \delta(x - x_r).$$

As an alternative, here we use the ED misfit function defined in the manner of Yuan et al. (2015):

$$\chi_E(m) = \frac{1}{2}\sum_{s,r}\int_0^T \left\| E_s(x_r,x_s,t;m) - E_d(x_r,x_s,t) \right\|^2 dt,$$

where E_s and E_d are the envelopes of synthetic and observed data, respectively. The corresponding adjoint source for a single source x_s can be formulated as:

$$f_E^\dagger(x,t) = \sum_r \left[E^{rat} s - H\{E^{rat} H s\} \right] \delta(x - x_r),$$

where E^{rat} measures the relative difference between synthetic and observed envelopes, namely

$$E^{rat} = \frac{E_s - E_d}{E_s}.$$

Injecting all adjoint sources simultaneously at all receiver locations generates the adjoint wavefield. The gradient is formed as a sum of all kernels, where each kernel is calculated from the zero-lag cross-correlation between the forward and adjoint wavefield for each individual event. In the next section we will show that the envelope misfit function designed in the described manner is a robust measure for highly nonlinear inversion of surface waves.

Synthetic example

We demonstrate our approach using the SEAM Phase II foothills model. To reduce the overall running time of the inversion, we select a portion of the original model. The selected volume is 7 x 3.5 x 3 km^3 in the X, Y and Z directions, respectively (Figure 1a). Topography contains strong variations (up to 900 m) and thus has a significant influence on recorded seismograms (e.g., Shin et al., 2013). The quality of the forward modelling in such challenging conditions with commonly used finite-difference (FD) methods will be strongly compromised because of staircase artifacts and inaccuracies related to the implementation of the free-surface condition. Here we prefer to use a spectral-element (SEM) solver, which, being based on a weak method, accurately captures topographic effects and naturally takes into account the free-surface condition. The mesh (Figure 1b) is constructed before the inversion and there is no need to rebuild it between the FWI iterations. Moreover, we found that the SEM modeling in case of a regular mesh (i.e., a mesh without distorted elements due to the presence of complex topography/bathymetry) is almost as efficient as our FD implementation (2nd order accurate in time and 4th order accurate in space) when a similar grid spacing is chosen for the two methods.

The true models contain strong variations in P and S wavespeeds and density. The variation in shear wavespeed in some locations is more than 1 km/s. This justifies our choice of a 3D elastic formulation, because the presence of strong elastic effects in observed data can significantly distort the inversion results if the acoustic approximation is used (e.g., Barnes and Charara, 2009; Borisov et al., 2015). Starting P wavespeed, S wavespeed, and density models were derived by smoothing the true model. For the inversion, we used 72 sources and 2,502 receivers regularly distributed on the surface. The distance between shots is 600 m in the X and Y directions, while the distance between receivers is 50 m and 200 m, respectively. Each source represents a force applied in the vertical direction with a Ricker wavelet as a source time function. To make the inversion more difficult, we use a relatively high frequency band (with a dominant frequency of 6 Hz) and we do not use a frequency multi-scale approach in the manner of Bunks et al. (1995) or Yuan et. al (2015). Furthermore, only the vertical component is used for all receivers. For the inversion, we used L-BFGS model updates with standard safeguards (e.g., Dennis and Schnabel 1996) that help provide numerical stability.

Figure 2 shows a comparison between the true, initial, and inverted models. At the initial stage we used the ED misfit function while inverting the entire content of the seismograms. After 30 iterations the S wavespeed model is significantly improved in the shallow part (Figures 2e and 2f). We used this result as input for the WD-FWI. After another 30 iterations the results show further refinements (Figures 2g and 2h). Source records for the shot located at x = 1 km, y = 1.75 km are shown in Figure 3. As the shallow part of the true model contains strong heterogeneities, the observed data are dominated by strong amplitude and dispersive Rayleigh surface waves. In contrast, the surface waves in the initial synthetics are much less dispersive because the starting model is relatively smooth. It is clear that the synthetic shot gather generated on a model inverted using envelope-based FWI agrees much more closely with the observed one. It is worth mentioning that the WD-FWI applied directly to the starting model (i.e., without ED-FWI) failed after a few unsuccessful trials of finding an adequate step length that reduces the misfit function.

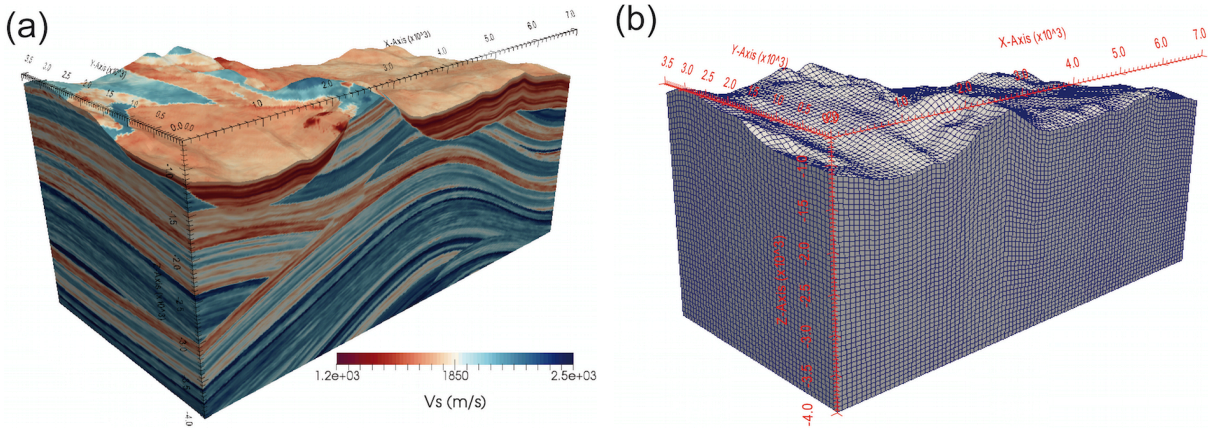

Figure 1: Portion of the 3D SEAM Phase II foothills model. Shear wavespeed (a) and the corresponding mesh (b).

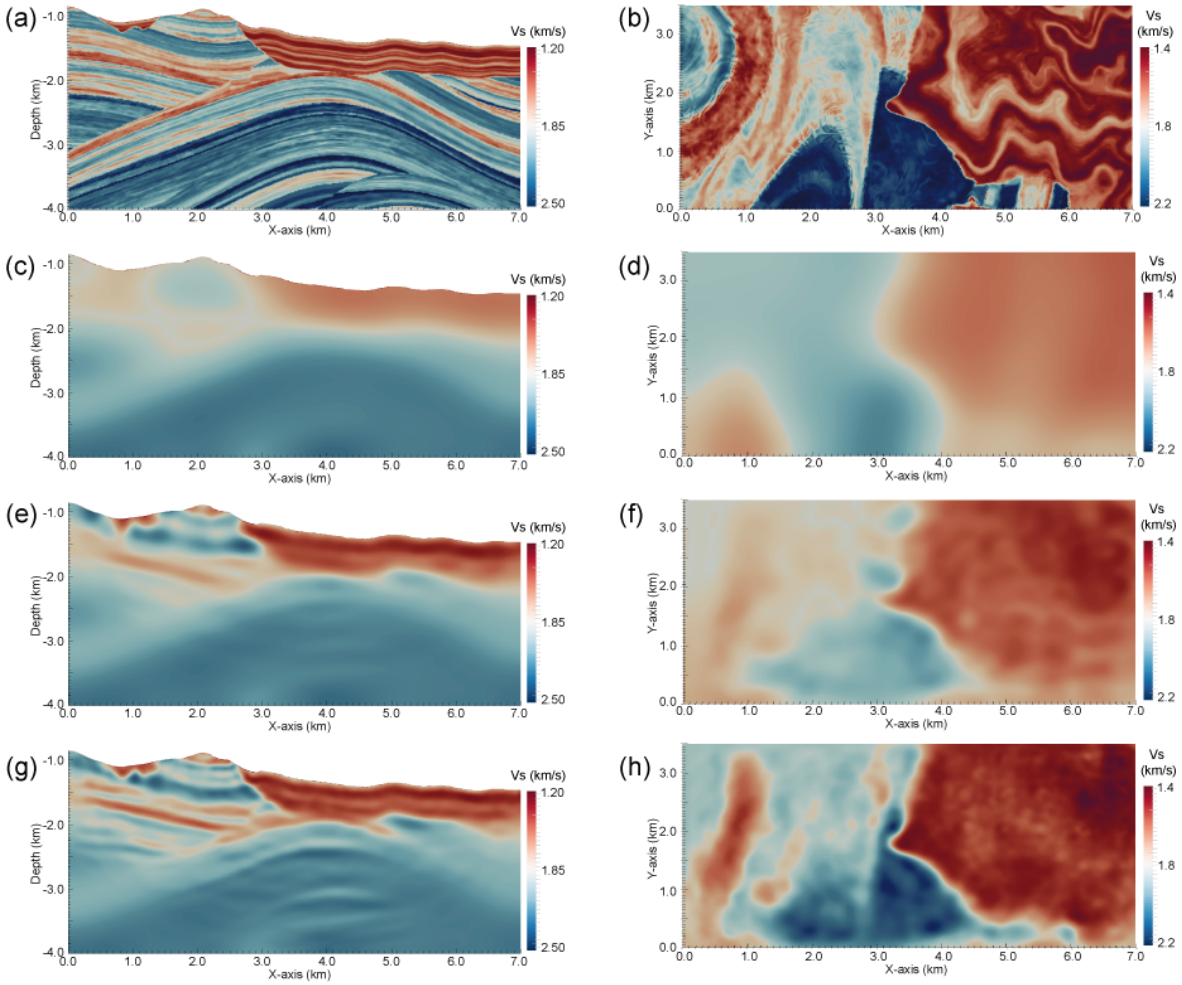

Figure 2: 3D elastic FWI results. Vertical slices (left) and horizontal slices at 1.7 km depth (right). True (a & b); initial (c & d); envelope-difference FWI (e & f); and waveform-difference FWI (g & h) models.

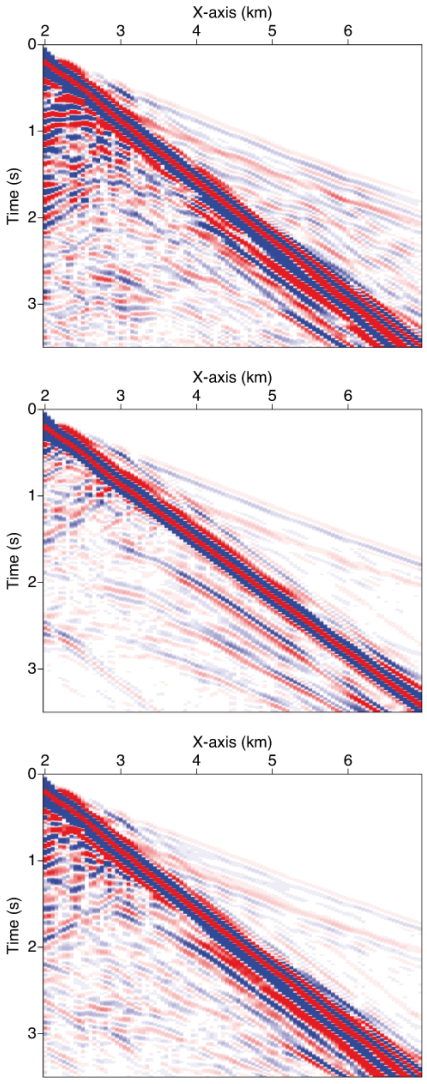

Figure 3: A shot record of the SEAM Phase II foothills model, vertical component of velocity: observed traces (top), initial synthetics (middle) and synthetics after envelope FWI (bottom).

If we zoom in on a single trace located at $x = 5.5$ km (Figure 4), we find that at this offset the surface waves are cycle-skipped, whereas the difference between the corresponding envelopes is not as pronounced. This assures that ED-FWI converges to a global minimum with higher probability.

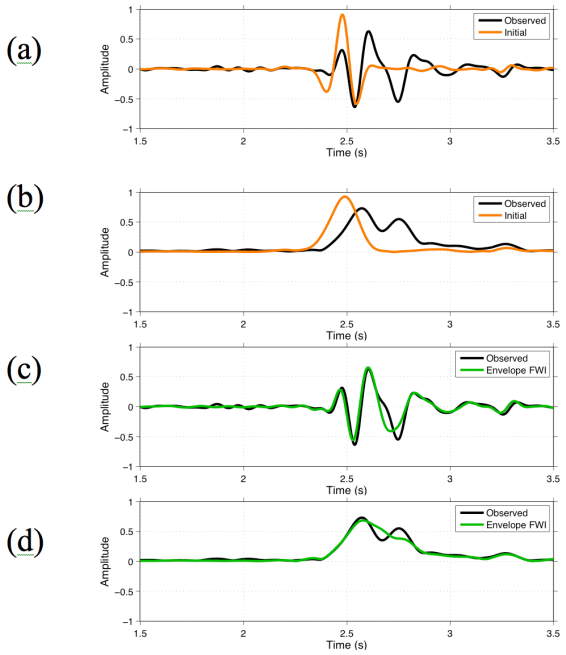

Figure 4: Trace comparisons from the shot record shown in figure 3. Trace located at x = 5.5 km: (a) observed trace and initial synthetics; (b) observed and initial envelopes; (c) observed trace and synthetic trace after envelope FWI; (d) observed and synthetic envelopes after envelope FWI.

Conclusions

We performed 3D elastic FWI of surface and body waves in the presence of strong wavespeed contrasts and variations in the topography. The envelope-based misfit function is shown to be effective for inverting surface waves, which are particularly exposed to the cycle-skipping problem. A synthetic example for the 3D SEAM Phase II foothills model illustrates that inversion of surface waves at the initial stages furnishes an improved starting shear wavespeed model for traditional FWI. Accurate wavefield modeling using 3D elastic spectral-element simulations is an important factor for a successful waveform inversion in such challenging geological settings.

Acknowledgments

The authors thank TOTAL S.A. for providing financial support and computational resources. We thank the SEAM consortium for providing the foothills model. The inversion was implemented using SeisFlows, a package developed by Ryan Modrak.

EDITED REFERENCES

Note: This reference list is a copyedited version of the reference list submitted by the author. Reference lists for the 2016 SEG Technical Program Expanded Abstracts have been copyedited so that references provided with the online metadata for each paper will achieve a high degree of linking to cited sources that appear on the Web.

REFERENCES

Barnes, C., and M. Charara, 2009, The domain of applicability of acoustic full-waveform inversion for marine seismic data: Geophysics, **74**, no. 6, WCC91–WCC103, http://dx.doi.org/10.1190/1.3250269.

Borisov, D., and S. C. Singh, 2015, Three-dimensional elastic full waveform inversion in marine environment using multi-component ocean-bottom cables: Synthetic study: Geophysical Journal International, **201**, 1215–1234, http://dx.doi.org/10.1093/gji/ggv048.

Bozdağ, E., J. Trampert, and J. Tromp, 2011, Misfit functions for full-waveform inversion based on instantaneous phase and envelope measurements: Geophysical Journal International, **185**, 845–870, http://dx.doi.org/10.1111/j.1365-246X.2011.04970.x.

Bunks, C., F. M. Saleck, S. Zaleski, and G. Chavent, 1995, Multiscale seismic waveform inversion: Geophysics, **60**, 1457–1473, http://dx.doi.org/10.1190/1.1443880.

Chavent, G., 1974, Identification of function parameters in partial differential equations: Joint Automatic Control Conference, **12**, 155–156, http://dx.doi.org/10.1109/JACC.1974.4170030.

Dennis, J. E., Jr., and R. B. Schnabel, 1996, Numerical methods for unconstrained optimization and nonlinear equations, 16: SIAM, http://dx.doi.org/10.1137/1.9781611971200.

Komatitsch, D., and J. P. Vilotte, 1998, The spectral element method: an efficient tool to simulate the seismic response of 2D and 3D geological structures: Bulletin of the Seismological Society of America, **88**, 368–392.

Komatitsch, D., and J. Tromp, 1999, Introduction to the spectral element method for three-dimensional seismic wave propagation: Geophysical Journal International, **139**, 806–822, http://dx.doi.org/10.1046/j.1365-246x.1999.00967.x.

Lailly, P., 1983, The seismic inverse problem as a sequence of before stack migrations, *in* J. B. Bednar, R. Redner, E. Robinson, and A.Weglein, eds., Conference on inverse scattering: Theory and application: SIAM, 206–220.

Oristaglio, M., 2012, SEAM update: The Leading Edge, **31**, 1130–1132, http://dx.doi.org/10.1190/tle31101130.1.

Tarantola, A., 1984, Inversion of seismic reflection data in the acoustic approximation: Geophysics, **49**, 1259–1266, http://dx.doi.org/10.1190/1.1441754.

Virieux, J., and S. Operto, 2009, An overview of full-waveform inversion in exploration geophysics: Geophysics, **74**, no. 6, WCC1–WCC26, http://dx.doi.org/10.1190/1.3238367.

Wu, R. S., J. Luo, and B. Wu, 2014, Seismic envelope inversion and modulation signal model: Geophysics, **79**, no. 3, WA13–WA24, http://dx.doi.org/10.1190/geo2013-0294.1.

Yuan, Y. O., F. J. Simons, and E. Bozdag, 2015, Multiscale adjoint waveform tomography for surface and body waves: Geophysics, **80**, no. 5, R281–R302, http://dx.doi.org/10.1190/geo2014-0461.1.